Temperature- and composition-driven changes in site occupation of indium solutes in $Gd_{1+3x}Al_{2-3x}$

Matthew O. Zacate and Gary S. Collins*
Department of Physics, Washington State University, Pullman, Washington 99164-2814, USA
(Received 2 September 2003; revised manuscript received 8 March 2004; published 25 May 2004)

Fractional concentrations of indium solutes at Gd sites and Al sites in the Laves phase $Gd_{1+3x}Al_{2-3x}$ were measured for different temperatures and sample compositions using perturbed angular correlation spectroscopy. At fixed composition, the fraction of indium on Gd sites was observed to decrease as temperature was increased. At fixed temperature, the fraction of indium on Gd sites was observed to increase as the composition became more deficient in Gd. The trends are explained using a thermodynamic model that couples solute site occupation with concentrations of point defects. The increase in enthalpy of the crystal when indium switches from a Gd site to an Al site was determined to be 0.343(7) eV.

DOI: 10.1103/PhysRevB.69.174202 PACS number(s): 61.72.Ss, 61.18.Fs, 82.60.Lf, 61.72.Ji

I. INTRODUCTION

There is considerable interest in the site occupation of solutes in intermetallic compounds because of its effects on many materials properties. Past experiments have shown that a solute may occupy different sites on opposing sides of the stoichiometric composition[1–4] and that a solute may change sites as a function of temperature.[5] Such results can be explained if concentrations of solutes on different sites are coupled with concentrations of intrinsic point defects. This is expected, as shown using a thermodynamic model of equilibrium site occupation in binary intermetallic compounds of any structure[6] results of which have been summarized recently.[4,7] Features highlighted in Refs. 4 and 7 have been noted in earlier simulations of solute site occupation carried out for NiAl,[8] TiAl,[9] and Ni_3Al.[10,11] In the present work, changes in site occupation of indium solutes in $GdAl_2$ were measured as a function of both composition and temperature using perturbed angular correlation of gamma rays (PAC) and analyzed using a thermodynamic model.

PAC is an attractive experimental technique for investigation of solute site occupation because it requires only very low concentrations of probes, used as solutes, which simplifies the thermodynamic analysis. Using PAC, characteristic interactions between the solute's nuclear quadrupole moment and electric field gradients (EFGs) in the crystal are used to determine the crystallographic locations of the solutes in some structures.

The EFG at a nucleus is the second derivative of the electrostatic potential due to the extranuclear charges in the surrounding crystal. The EFG is a traceless, second-order tensor V_{ij}, which in diagonal form has components customarily ordered so that $|V_{zz}| \geqslant |V_{yy}| \geqslant |V_{xx}|$. The two independent parameters usually reported are the principal component V_{zz} and the asymmetry parameter $\eta \equiv (V_{xx} - V_{yy})/V_{zz}$. For nuclei at a site with cubic site symmetry, the EFG is zero ($V_{zz}=0$ and $\eta=0$). For sites with a threefold axis of symmetry (for example, $\bar{3}m$ site symmetry), $V_{zz} \neq 0$ and $\eta=0$. For lower symmetry, $V_{zz} \neq 0$ and $0 < \eta \leqslant 1$. V_{zz} and η can be used to distinguish sites and provide limited information about point symmetries of the sites.

Changes in solute site occupation have been observed using PAC in previous studies. Indium solute site occupation was found to vary as a function of composition in Ni_2Ga_3 and other phases having the Ni_2Al_3 structure.[3,4] Site occupation of indium was observed to change as a function of temperature in $HfAl_2$.[5] Changes in site occupation of hafnium with temperature were observed in $LiNbO_3$ and $LiTaO_3$, and the changes were analyzed using a thermodynamic model coupled to intrinsic defects.[12]

The present study in $GdAl_2$ demonstrates changes in site occupation of indium as functions of both composition and temperature. $GdAl_2$ is a cubic Laves phase having the Cu_2Mg (C15) structure.[13] It has several features that suggested one might observe changes in site occupation by indium solutes. First, one can easily distinguish the two sites using PAC because the Gd site has $\bar{4}3m$ (cubic) site symmetry while the Al site has $\bar{3}m$ (axial) site symmetry. Second, indium is isovalent with Gd and Al, suggesting that it would not have a strong chemical preference for either site. Third, the atomic volume of In is intermediate between volumes of Gd and Al, suggesting that there would not be a large difference in strain energy if In were to substitute at one site versus the other.

$GdAl_2$ is thought to disorder by formation of thermally activated "quadruple defects," comprised of three aluminum vacancies (V_{Al}) and one aluminum antisite (Al_{Gd}).[14] These were the defects observed using x-ray diffraction, ac magnetic susceptibility, and dc magnetization after high-energy ball milling.[14] The formation energy of quadruple defect disorder was estimated to be 0.57 eV per defect and to be lowest of all types of disorder using Miedema's semiempirical model.[15] $GdAl_2$ appears as a line compound in the Gd–Al phase diagram,[16] however, as for all compounds, its phase field must have a finite, though possibly very small, width. Therefore, the compound is better represented by the formula $Gd_{1+3x}Al_{2-3x}$, in which x denotes the deviation from the stoichiometric composition. Since formation enthalpies of the neighboring $GdAl_3$ and GdAl phases at room temperature are both higher than that of $Gd_{1+3x}Al_{2-3x}$,[17,18] the phase field of $Gd_{1+3x}Al_{2-3x}$ should extend to both sides of the stoichiometric composition. This suggested to us that we

could prepare $Gd_{1+3x}Al_{2-3x}$ samples with Gd-poor and Gd-rich compositions and study solute site occupation as a function of composition as well as temperature.

II. EXPERIMENTAL METHODS

A. Sample preparation

Gd-Al samples with compositions between about 25.7 at. % Gd and 34.0 at. % Gd were prepared by arc melting 99.9% Gd foil and 99.997% Al foil with carrier-free ^{111}In under Ar atmosphere. Indium concentrations were very dilute (about 10^{-7} at. %). Samples were annealed at 1273 K for 2–4 h either in vacuum better than 10^{-6} mbar or in flowing 99.9995% H_2 before measurement to anneal out excess defects and increase grain size. Observed PAC signals and site occupation behavior did not appear to depend on annealing treatment. PAC signals exhibited only small frequency distributions, which indicated that the treatments resulted in well crystallized and ordered crystals having low concentrations of point defects.

Samples labeled *A* through *F* were prepared with nominal compositions of 32.5, 33.3, 33.5, 33.3, 34.3, and 33.7 at. % Gd. Typically, about 0.1 mg was lost out of a total mass of about 35 mg during each melt, and uncertainties in compositions of the melted samples were determined by assuming that decreases in mass were due entirely to loss of one element or the other. Samples *C* and *E* gained 0.15 mg during anneals in H_2, which is attributed to oxidation of Gd by impurity oxygen in the hydrogen.[19] Compositions of those two samples were adjusted according to the amounts of Gd lost from the intermetallic phase. Considering the above effects, best estimates for compositions of samples *A* through *F* as measured are $32.5^{+0.7}_{-0.2}$, $33.3^{+0.2}_{-0.1}$, $32.7^{+0.3}_{-0.1}$, $33.3^{+0.2}_{-0.1}$, $33.5^{+0.4}_{-0.1}$, and $33.7^{+0.3}_{-0.1}$ at. % Gd. The width of the $Gd_{1+3x}Al_{2-3x}$ phase field, which has not been determined, may be so narrow that some samples were in two-phase fields, containing small volume fractions of neighboring phases. A $GdAl_3$ sample [25.7(1) at. % Gd] was therefore prepared to check if any signals observed in the present work were from that compound.

B. Perturbed angular correlation spectroscopy

Crystallographic locations of indium were identified using gamma radiation emitted from ^{111}In/Cd probes dissolved in $Gd_{1+3x}Al_{2-3x}$. ^{111}In decays to the second excited state of ^{111}Cd via electron capture. The Cd nucleus subsequently decays to its ground state by emitting two gamma rays in succession. The intermediate 247 keV level has spin $5/2^+$ and a long lifetime, $\tau = 120$ ns. For such a cascade, there is an anisotropic probability of detecting the second gamma ray of the cascade with respect to the first gamma ray's direction of detection. When an EFG is present at the Cd nucleus, the system is perturbed and populations of the magnetic substates of the 247 keV level evolve over the lifetime of the level. As a result, there is a time dependence in the angular correlation between the gamma rays of the cascade that is characterized by a perturbation function $G_2(t)$.

The time evolution of the magnetic substates is analogous to spin precession in a magnetic field. For a spin-5/2 nuclear quadrupole interaction, there are three interaction frequencies ω_1, ω_2, and $\omega_3 = \omega_1 + \omega_2$, which are functions of the magnitude of electric field gradient V_{zz} and η.[20] For $\eta = 0$, the frequencies are $\omega_1 \equiv 3eQV_{zz}/20\hbar$ where Q is the quadrupole moment of the nucleus, $\omega_2 = 2\omega_1$, and $\omega_3 = 3\omega_1$. When EFG axes are randomly oriented, as for polycrystalline samples such as the $Gd_{1+3x}Al_{2-3x}$ samples of this study, the perturbation function is

$$G_2(\omega_1, \eta, \sigma, t) = s_0 + \sum_{n=1}^{3} s_n \cos(\omega_n t) \exp\left(-\frac{1}{2}(\sigma \omega_n t/\omega_1) \right). \quad (1)$$

In general, the amplitudes s_n are functions of η. For most signals observed in this study, $\eta = 0$, in which case $s_0 = 1/5$, $s_1 = 13/35$, $s_2 = 2/7$, and $s_3 = 1/7$.[20] The exponential factors account for inhomogeneous broadening due to distant defects or lattice strains.

When nuclei are located in more than one crystallographic environment, the overall perturbation function is a superposition of individual functions,

$$G_2(t) = \sum_i f_i G_2(\omega_{1,i}, \eta_i, \sigma_i, t), \quad (2)$$

in which the signal amplitude f_i is the fraction of nuclei in site *i*. The hyperfine parameters $\omega_{1,i}$ and η_i identify the crystallographic site, and the site fractions f_i are direct measures of site occupation. While hyperfine interactions are measured in the 247 keV level of Cd, the site fractions are determined by the equilibrium distribution of In, since there is not enough time after the decay of In for Cd to jump to a different site. Hyperfine parameters and site fractions were determined by least squares fits of Eqs. (1) and (2) to experimental spectra.

Data were collected using a PAC spectrometer with four fixed BaF_2 scintillation detectors separated by 90° in a plane. Measurements at elevated temperature were made in vacuum better than 10^{-6} mbar in a furnace designed to minimize sample-detector distance.[21] The spectrometer used a slow–fast coincidence counting method with ''nongated'' timing signals.[22] Data reduction took into account correlated absorption of gamma rays in the source, which primarily leads to a vertical offset in the perturbation function,[23–25] and attenuation at high count rates.[22] These artifacts were removed from all spectra prior to analysis, and only corrected spectra are shown. A detailed description of the data reduction methodology can be found in Ref. 22.

III. RESULTS

PAC spectra for four $Gd_{1+3x}Al_{2-3x}$ samples measured at 823 K are shown in Fig. 1. The spectrum for sample *F* [Fig. 1(a)] exhibits only one quadrupole interaction signal with fundamental frequency $\omega_1 = 45$ Mrad/s. The spectrum for sample *D* [Fig. 1(b)] exhibits, in addition to the 45 Mrad/s signal, a 0 Mrad/s signal visible as a small vertical offset. In the spectrum for sample *B* [Fig. 1(c)], the site fraction of the

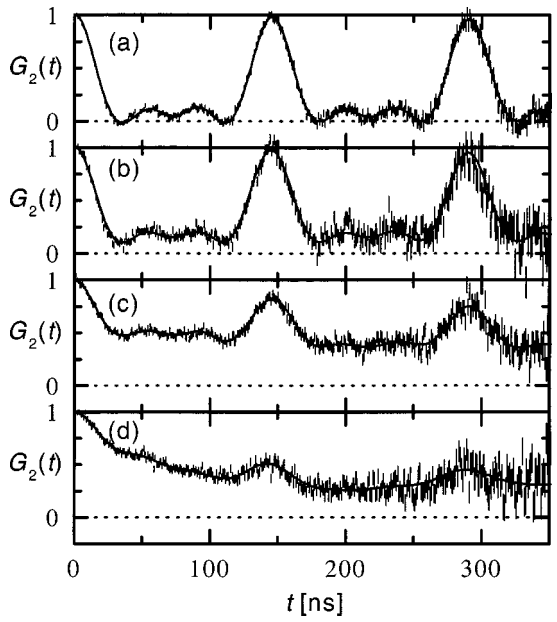

FIG. 1. PAC spectra of ^{111}In/Cd in $Gd_{1+3x}Al_{2-3x}$ samples of different compositions measured at 823 K: samples *F* (a), *D* (b), *B* (c), and *A* (d). The compositions vary from being nearly stoichiometric in (a) to Gd poor in (d).

45 Mrad/s signal is half replaced by two signals: the 0 Mrad/s signal and an 8 Mrad/s signal. Finally, the spectrum for sample *A* [Fig. 1(d)] exhibits the smallest site fraction of the 45 Mrad/s signal, accompanied by 0 Mrad/s, 8 Mrad/s, and 14 Mrad/s signals. The site fractions in the samples are correlated with composition: the site fraction of the 45 Mrad/s signal is highest for sample *F*, which is Gd rich, and lowest for sample *A*, which is Gd poor. Because of large uncertainties in the compositions of the samples, the samples were labeled $A-F$ according to the progressive increase in site fraction of the 45 Mrad/s signal at a given temperature. This is believed to give a better ordering of the actual compositions in terms of increasing Gd content than the nominal compositions, as discussed below.

A PAC measurement was carried out on a sample of the neighboring phase $GdAl_3$ to check if the 0 Mrad/s, 8 Mrad/s, or 14 Mrad/s signals originate from that phase. The spectrum, shown in Fig. 2, exhibits only a single signal with $\omega_1 = 61.5(1)$ Mrad/s and $\eta = 0.13(1)$, which differs from all signals observed in $GdAl_2$. It is worth noting that this implies a strong site preference of indium solutes in $GdAl_3$. $GdAl_3$ has the Ni_3Sn structure, in which the Gd site has $\bar{6}m2$ (axial) symmetry and the Al site has $mm2$ (nonaxial) symmetry.[13] Observation of a single signal with a nonzero value of η indicates a strong preference of indium for the Al site.

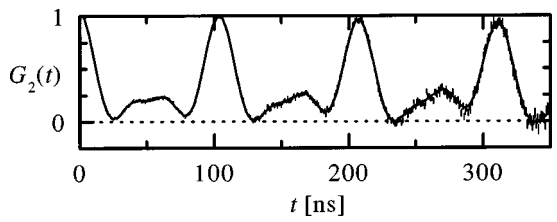

FIG. 2. PAC spectrum of ^{111}In/Cd in $GdAl_3$ measured at room temperature.

The 45 Mrad/s signal was identified with In/Cd probes on Al sites in previous PAC studies of $GdAl_2$,[26–28] with no signal reported in those studies for probes on Gd sites. In the present study, the 0 Mrad/s signal can only come from probes on the cubic Gd site. The site fraction of the 0 Mrad/s signal is highest for sample *A*, which is Gd poor, and the signal was not observed for sample *F*, which is Gd rich. Thus, the site fraction of the 0 Mrad/s signal increases with decreasing Gd content, whereas the site fraction of the 45 Mrad/s signal decreases with decreasing Gd content.

The site fraction of the 8 Mrad/s signal, like that of the 0 Mrad/s signal, was observed to increase with decreasing Gd content. Because the concentration of structural defects for Gd-poor compositions also increases as Gd-content decreases, the 8 Mrad/s most likely arises from probes that have a nearby structural defect.[29] Possible structural defects are the Al antisite defect Al_{Gd} or the Gd vacancy V_{Gd}, both located on the Gd sublattice.

The low frequency of the 8 Mrad/s signal indicates that it originates from probes on Gd sites and not on Al sites, as follows. Typical interaction frequencies for Cd probes at cubic sites in other metallic systems with a defect in a nearest neighbor site are in the range of 50 to 100 Mrad/s,[30] significantly higher than 8 Mrad/s. A small EFG with a corresponding low frequency might in principle be caused by cancellation of most of the EFG at a probe on the Al site by a defect at a first neighbor Gd site. This possibility was investigated by carrying out point charge calculations of EFGs in which a range of effective charges were considered for the defect. We found that the frequency could be decreased by at most only 2% because of the particular angle between the EFG axis of the defect-free Al site and the EFG axis arising from the defect at a neighboring Gd site. Thus, the 8 Mrad/s signal cannot be explained by the hypothesis that the probe lies at an Al site, and must be attributed to probes on Gd sites, which have cubic symmetry. While an 8 Mrad/s frequency would be low for a defect in the first neighbor shell of the otherwise cubic Gd site, defects in Gd-poor $Gd_{1+3x}Al_{2-3x}$ are located on Gd sites, and the closest Gd sites are second, not first, neighbors. The low frequency is consistent with a defect in a more distant site, because an EFG (or interaction frequency) is inversely proportional to the cube of the distance between a probe and defect. This is illustrated well in PAC experiments in B2 compounds, for which frequencies of signals arising from defects at second neighbor distances were found to be only 15% to 34% as large as frequencies of signals arising from defects at first neighbor distances.[31]

Therefore, the 8 Mrad/s signal comes from probes on Gd sites with a defect on the closest Gd site. Based on the PAC signals alone, one cannot distinguish whether the Gd-poor defect is V_{Gd} or Al_{Gd}. Since other studies indicate that Al_{Gd} is the Gd-poor structural defect,[14] the 8 Mrad/s signal most likely comes from probes on Gd sites with an Al_{Gd} defect at a nearby Gd site.

The 14 Mrad/s signal was observed only in spectra for

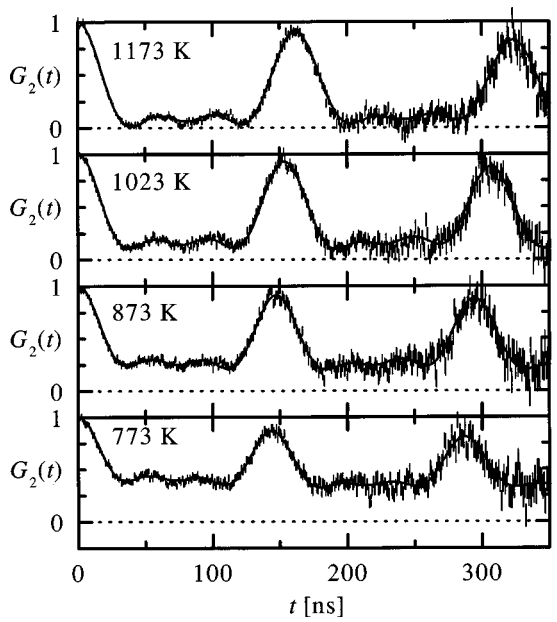

FIG. 3. PAC spectra of ^{111}In/Cd in $Gd_{1+3x}Al_{2-3x}$ sample *C* measured at the indicated temperatures.

sample *A*. Because sample *A* was the most Gd poor of all samples, it is reasonable to conclude that, like the 8 Mrad/s signal, the signal also involves the Gd-poor structural defect. One possibility is that the 14 Mrad/s signal arises from multiple Al_{Gd} defects near Cd_{Gd} probes, in analogy with multiple vacancy configurations that have been detected around probes in B2 compounds.[31–33] However, it was not possible to identify the 14 Mrad/s signal more positively.

In Fig. 3, representative PAC spectra collected for sample *C* at different temperatures are shown. The site fraction of the 0 Mrad/s signal, visible as a vertical offset in each spectrum, can be seen to decrease with increasing temperature with a compensating increase in the fraction of the signal with frequency of about 45 Mrad/s. This trend shows that indium tends to occupy Gd sites at low temperature and Al sites at high temperature.

It is evident in Fig. 3 that the frequency of the signal for Cd on the Al site decreases with increasing temperature, which is attributed in part to thermal expansion. Figure 4 shows a plot of the temperature dependence of the frequency ω_1 for all samples, in which it can be seen that the frequencies for different samples overlap excellently. A linear fit of data for all samples (excluding sample *A*, which had larger errors) yielded $\omega_1 = 48.8(3)$ Mrad/s at room temperature and $d\omega_1/dT = -0.0109(3)$ Mrad/s/K. Below, this signal is labeled the 49 Mrad/s signal, in reference to its frequency at room temperature. Hyperfine parameters and site attributions of all signals are summarized in Table I.

Major conclusions from the above discussion are that the site fraction of the 0 Mrad/s signal f_0 corresponds to f_{Gd}, the fraction of probes on Gd sites without nearby defects, and that the site fraction of the 49 Mrad/s signal f_{49} corresponds to f_{Al}, the fraction of probes on Al sites. For analysis using a thermodynamic model, it is useful to make an Arrhenius plot of f_0/f_{49}, shown in Fig. 5 for samples $A-E$. (The ratios

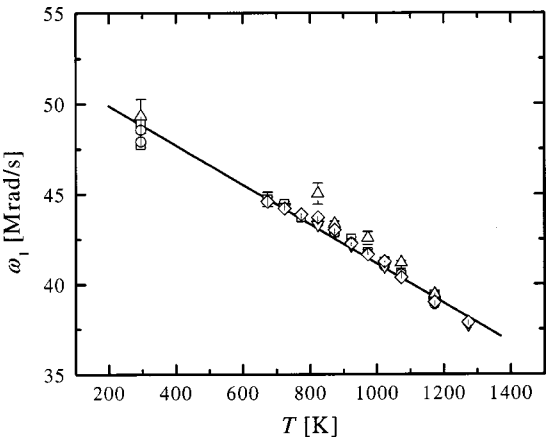

FIG. 4. Temperature dependence of the quadrupole interaction frequency ω_1 of ^{111}Cd on the Al site for all six $GdAl_2$ samples. The line shows the result of a linear fit to data for all samples except sample *A* (up triangles).

of site fractions for sample *F* were consistent with zero in all measurements and are not visible in the figure.) As can be seen, indium tends to occupy Gd sites at low temperature and Al sites at high temperature in each of the five samples.

The temperature dependences of the site fractions of the 8 Mrad/s signal f_8, attributed to a probe on a Gd site with a nearby defect, and of the 0 Mrad/s signal f_0, attributed to a probe on a Gd site without a nearby defect, can in principle be used to determine the interaction energy between the probe and defect. For this, it is useful to construct an Arrhenius plot of the ratio f_8/f_0, shown in Fig. 6 for samples *B* and *C* (ratios for other samples had large scatter). The ratios can be seen to increase as the temperature decreases, indicating an attractive interaction between the Gd-poor structural defect and the indium probe.

IV. THERMODYNAMIC ANALYSIS OF SITE OCCUPATION

A thermodynamic model was employed to interpret the temperature and composition dependence of the data in Fig. 5 (see Appendix). The model links indium concentrations on each sublattice of $Gd_{1+3x}Al_{2-3x}$ to the concentrations of intrinsic defects. Defects are assumed to be present only in small concentrations and to be noninteracting. The effect of interaction between In_{Gd} and the structural defect of Gd-poor compositions is considered separately in the next section. In accordance with conclusions of Bakker and co-workers,[14,15] the dominant defects are assumed to be Al_{Gd} and V_{Al}, and other defect concentrations were neglected.

One way to link changes in indium site occupation to intrinsic defects is via the reaction

$$In_{Gd} + Al_{Al} \rightleftarrows In_{Al} + Al_{Gd}, \tag{3}$$

which describes the partitioning of indium between Al and Gd sites in equilibrium. Application of the law of mass action to Eq. (3) relates the ratio of indium concentrations on each site to the Al_{Gd} concentration via

TABLE I. Hyperfine signals observed for ^{111}In/Cd probes in $GdAl_2$.

ω_1 at 300 K (Mrad/s)	$d\omega_1/dT$ (Mrad/s/K)	η	Probe site	Nearby defects
48.8(3)	−0.0109(3)	0	Al	None
0		0	Gd	None
8(1)	−0.0022(16)	0	Gd	One closest neighbor Al_{Gd}
14.2(3)	−0.00(2)	0.27(3)	Gd	Two closest neighbors Al_{Gd}

$$\frac{[\mathrm{In_{Al}}][\mathrm{Al_{Gd}}]}{[\mathrm{In_{Gd}}][\mathrm{Al_{Al}}]} = \exp(-G_{\mathrm{xfer}}/k_BT) = \exp(-(g^{\mathrm{In}}_{\mathrm{Al}} - g^{\mathrm{In}}_{\mathrm{Gd}} + g^{\mathrm{Al}}_{\mathrm{Gd}})/k_BT), \quad (4)$$

in which bracketed quantities $[X_y]$ are fractions of sublattice y occupied by species X. $G_{\mathrm{xfer}} = H_{\mathrm{xfer}} - TS_{\mathrm{xfer}}$ is the change in free energy of the crystal when indium transfers from the Gd site to the Al site and includes changes in enthalpy H_{xfer} and vibrational entropy S_{xfer}. As shown in the Appendix, G_{xfer} is related to individual free energies of defects g^X_y.

The ratio of site fractions is defined in terms of solute concentrations as $f_0/f_{49} = f_{\mathrm{Gd}}/f_{\mathrm{Al}} = \frac{1}{2}[\mathrm{In_{Gd}}]/[\mathrm{In_{Al}}]$, in which the factor 1/2 is the ratio of the numbers of sites on the Gd and Al sublattices. Using this expression in conjunction with Eq. (4), one obtains for the ratio of site fractions

$$f_0/f_{49} = \tfrac{1}{2}[\mathrm{Al_{Gd}}]\exp(-S_{\mathrm{xfer}}/k_B)\exp(H_{\mathrm{xfer}}/k_BT). \quad (5)$$

Thus, the site fraction ratio is directly proportional to the concentration of Al_{Gd}. The temperature and composition dependence of $[Al_{Gd}]$ and consequent behavior of the site fraction ratio are discussed in the Appendix.

Below approximately 673 K, the ratios in Fig. 5 are independent of temperature, indicating that the samples were unable to establish equilibrium through defect motion on the time scale of the measurements. At and above 673 K, the ratios of site fractions exhibit reversible, activated behavior. The slopes of the data in Fig. 5 are similar for samples $A-E$,

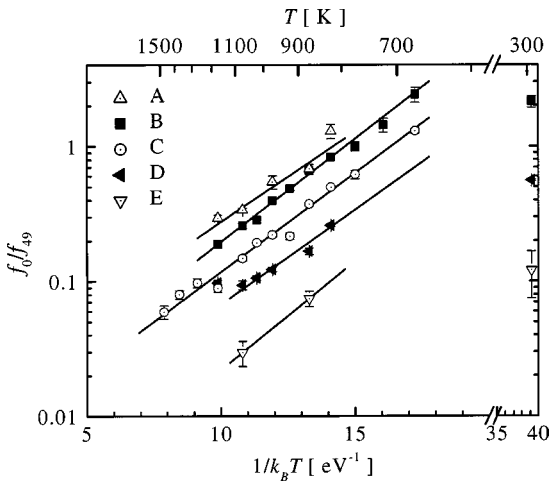

FIG. 5. Ratios of fractions of indium on Gd and Al sites, f_0/f_{49}, plotted versus inverse temperature for samples $A-E$. Straight lines show results of fits to Eq. (6) to determine H_{xfer} and S_{xfer}.

indicating samples $B-E$ are also Gd poor like sample A; however, the samples have different compositions as indicated by offsets in ratios for the samples. Up to the highest measured temperature, 1473 K, there is no clear evidence of curvature in the ratios, which would have indicated formation of thermally activated defects. Based on these observations we conclude that the samples were sufficiently Gd poor for structural Al_{Gd} to dominate over any thermally activated Al_{Gd}, in which case $[Al_{Gd}] \cong -3x$ (see the Appendix). Hence, the data in Fig. 5 can be interpreted using

$$f_0/f_{49} = -\frac{3x}{2}\exp(-S_{\mathrm{xfer}}/k)\exp(H_{\mathrm{xfer}}/k_BT), \quad (6)$$

and the temperature dependence of f_0/f_{49} is due entirely to the Boltzmann factor involving H_{xfer}.

Data for samples A, B, C, D, and E were fitted to Eq. (6), with results shown by lines in Fig. 5. Values for H_{xfer}, obtained from the slopes, and for the products $-\frac{3}{2}x\exp(-S_{\mathrm{xfer}}/k_B)$, obtained from the intercepts at $1/k_BT = 0$, are listed in Table II. H_{xfer} is an intrinsic property of the transfer process and therefore should be the same for all samples. The average value is $H_{\mathrm{xfer}} = 0.343(7)$ eV. S_{xfer} should also be the same for all samples; thus, in principle one can determine S_{xfer} from the fitted intercepts using the deviations from stoichiometry. Unfortunately, the large uncertainties of the compositions of the samples do not allow a meaningful determination of S_{xfer} to be made.

One can, however, determine the relative deviations from stoichiometry for samples $A-E$. For example, one could take ratios of the fitted intercepts to obtain the relative deviations from stoichiometry for samples $A-E$. A more accurate determination was made by using the actual f_0/f_{49} data rather than the fitted intercepts. Because the range of probable composition for sample A was entirely Gd poor, the deviations from stoichiometry for the other samples were found relative to that of sample A. The ratio of deviation from stoichiometry of sample n to that of sample A was determined using the corresponding site fraction ratio at a given temperature; that is,

$$\frac{x_n}{x_A} = \frac{(f_0/f_{49})_{\text{sample } n \text{ at } T}}{(f_0/f_{49})_{\text{sample } A \text{ at } T}}. \quad (7)$$

Ratios x_n/x_A were calculated from all available pairs of f_0/f_{49} for temperatures at which samples n and A were both measured and then averaged for each sample, yielding $x_B/x_A = 0.75(13)$, $x_C/x_A = 0.42(9)$, $x_D/x_A = 0.26(5)$, and $x_E/x_A = 0.10(2)$.

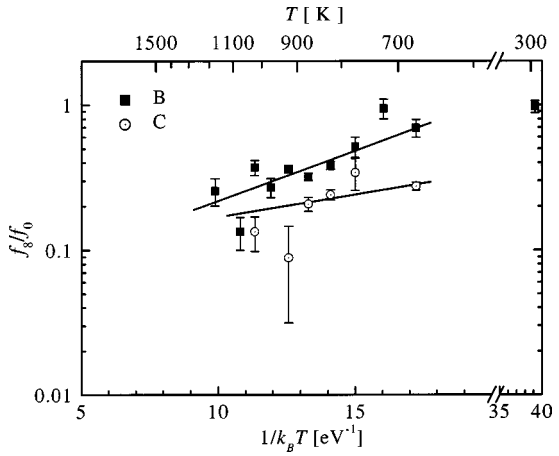

FIG. 6. Ratios of fractions of indium on defect-associated and defect-free Gd sites, f_8/f_0, plotted versus inverse temperature for samples *B* and *C*. Straight lines show results of fits to Eq. (10) to determine H_B and S_B.

To illustrate more clearly changes in site occupation as a function of composition, fractions of probes on Al sites are plotted in Fig. 7 versus the relative deviation from stoichiometry $x/|x_A|$ for several temperatures. For each temperature, the Al-site fraction decreases as the magnitude in the deviation from stoichiometry increases. Overall changes in site fractions from a composition near the stoichiometric composition (sample *E*) to sample *A* are observed to be as large as 80% at low temperatures (at and below 673 K), decreasing to about 20% in measurements at high temperatures (1073 and 1173 K). Based on the nominal composition of sample *A*, these changes take place over a composition range of roughly 0.8 at. % Gd. The changes are consistent with heuristic rules identified from a more extensive examination of the thermodynamic model of site occupation, including simulations.[4,6,7] In particular, a solute tends to occupy the lattice site of an element in which a compound is deficient. This is seen in Fig. 7 as a decrease in f_{49}, which corresponds to an increase in occupation of Gd sites by indium, as Gd content decreases.

V. THERMODYNAMIC ANALYSIS OF DEFECT ASSOCIATION

Assuming for concreteness that Al_{Gd} is the Gd-poor structural defect, the interaction enthalpy between Al_{Gd} and the In_{Gd} probe can be determined from the ratio of the 0 Mrad/s and 8 Mrad/s site fractions. Since the concentration of Al_{Gd} is small, one can write the reaction for binding (or disassociation) as

$$\{In_{Gd}:Al_{Gd}\} \rightleftarrows In_{Gd} + Al_{Gd}, \tag{8}$$

in which $\{In_{Gd}:Al_{Gd}\}$ denotes a bound pair of defects. Using the law of mass action, the concentrations of defects in Eq. (8) are related according to

$$z\frac{[In_{Gd}][Al_{Gd}]}{[In_{Gd}:Al_{Gd}]} = \exp(-G_B/k_BT), \tag{9}$$

TABLE II. Sample compositions and transfer enthalpies and intercepts fitted using Eq. (6).

Sample	Composition (at. % Gd)	x	H_{xfer} (eV)	$-\frac{3}{2}x\exp(-S_{xfer}/k_B)$
A	$32.5^{+0.7}_{-0.2}$	$-0.008^{+0.7}_{-0.2}$	0.31(5)	0.012(6)
B	$33.3^{+0.2}_{-0.1}$	$0.000^{+0.2}_{-0.1}$	0.35(1)	0.0058(9)
C	$32.7^{+0.3}_{-0.1}$	$-0.006^{+0.3}_{-0.1}$	0.34(1)	0.0040(7)
D	$33.3^{+0.2}_{-0.1}$	$0.000^{+0.2}_{-0.1}$	0.32(3)	0.0026(9)
E	$33.5^{+0.4}_{-0.1}$	$0.002^{+0.4}_{-0.1}$	0.4(3)	0.0005(10)
F	$33.7^{+0.3}_{-0.1}$	$0.004^{+0.3}_{-0.1}$		

in which the free energy of binding is $G_B = H_B - TS_B$ and $z = 4$ is the number of neighboring Gd sites closest to a Gd site. $H_B > 0$ indicates an attraction between neighboring defects. The ratio of the site fractions f_8/f_0 is equal to the ratio of concentrations of bound and unbound indium probes on Gd sites: $[In_{Gd}:Al_{Gd}]/[In_{Gd}]$. Since the concentration $[Al_{Gd}]$ was found to be independent of temperature for each sample and equal to $-3x$, one has the following relation between the site fraction ratio and temperature:

$$\frac{f_8}{f_0} = -12x\exp(-S_B/k_B)\exp(+H_B/k_BT). \tag{10}$$

Ratios for samples *B* and *C* shown in Fig. 6 were fitted to the function in Eq. (10), from which $H_B = 0.16(4)$ eV and $H_B = 0.07(3)$ eV for samples *B* and *C*, respectively, with an average value $H_B = 0.12(6)$ eV.

VI. DISCUSSION

Qualitative trends of indium site occupation in $Gd_{1+3x}Al_{2-3x}$ are independent of the actual structural defect that is dominant in Gd-poor samples. One can readily recast the site-occupation model under the assumption that V_{Gd} is the dominant structural defect in Gd-poor samples, leading to

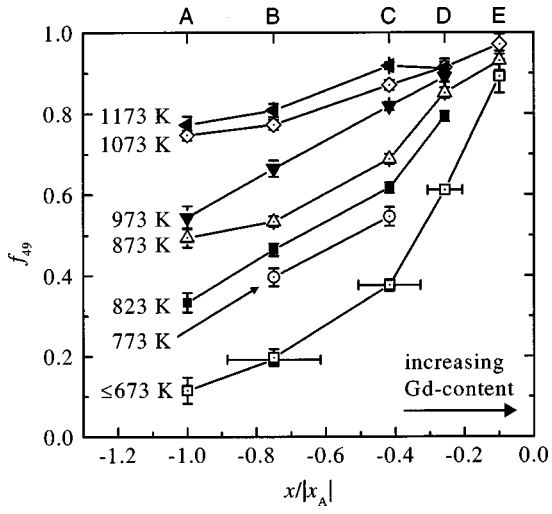

FIG. 7. The fraction of solutes occupying Al sites (with frequency 49 Mrad/s) for samples $A-E$, plotted versus relative deviation from stoichiometry $x/|x_A|$ at the indicated temperatures.

$f_{\mathrm{Gd}}/f_{\mathrm{Al}}=\frac{1}{2}[\mathrm{V_{Gd}}]^{3/2}\exp(-S_{\mathrm{xfer}}/k_B)\exp(H_{\mathrm{xfer}}/k_BT)$, with $[\mathrm{V_{Gd}}]\cong -9x/2$ for Gd-poor compositions in which there is little thermal activation of $\mathrm{V_{Gd}}$ defects. The physical interpretation to be given to the activation enthalpy $H_{\mathrm{xfer}}=0.343(7)$ eV would differ, with $H_{\mathrm{xfer}}=h^{\mathrm{In}}_{\mathrm{Al}}-h^{\mathrm{In}}_{\mathrm{Gd}}+\frac{3}{2}h^{V}_{\mathrm{Gd}}+\frac{1}{2}h_0$ instead of $H_{\mathrm{xfer}}=h^{\mathrm{In}}_{\mathrm{Al}}-h^{\mathrm{In}}_{\mathrm{Gd}}+h^{\mathrm{Al}}_{\mathrm{Gd}}$. Similarly, interpretation of the data for defect association between indium and the Gd-poor defect would be affected by a different identity for the Gd-poor structural defect, but the $H_B=0.12(6)$ eV would remain the same. Quantitatively, relative deviations from stoichiometry x_n/x_A would differ because of the 3/2-power dependence on $[\mathrm{V_{Gd}}]$.

VII. SUMMARY AND CONCLUSION

Fractional concentrations of indium solutes at Gd and Al sites in $\mathrm{Gd_{1+3x}Al_{2-3x}}$ were measured as a function of temperature and composition using perturbed angular correlation spectroscopy. The fraction at Al sites was found to increase with either increasing temperature or Gd content. The transfer of an indium solute from the gadolinium to aluminum sublattice was found to increase the enthalpy of the crystal by 0.343(7) eV. In addition, indium solutes on Gd sites were found to have an attractive interaction with the Gd-poor structural defect, with a binding enthalpy of 0.12(6) eV.

Indium was observed to switch almost completely from Gd to Al sites in response to changes in temperature of order 400 K or changes in composition of order 0.8 at.% Gd. Similarly large changes in solute site occupation may occur in other compounds and significantly influence material properties. Without thorough investigation of site occupation as a function of composition and temperature, one risks an incomplete assessment of site preference behavior, such as identification of one preferred site to the exclusion of other sites. Many phases that appear as line compounds in binary phase diagrams are likely to have widths of phase fields comparable to that of $\mathrm{GdAl_2}$, so that composition dependences may be as great as in the present study. At a minimum, one should investigate a reported line compound by preparing samples to be rich or poor in each element in order to observe site preferences at the opposing boundary compositions.

ACKNOWLEDGMENT

This work was supported in part by the National Science Foundation under Grant No. DMR 00-91681 (Metals Program).

APPENDIX

Equilibrium concentrations of intrinsic defects and solutes on the various sublattices of a crystal can be determined by minimizing the Gibbs free energy of the crystal subject to structural and compositional constraints within the framework of a canonical ensemble. This method is used below to determine the composition and temperature dependence of indium solute site occupation and intrinsic defect concentrations in $\mathrm{Gd_{1+3x}Al_{2-3x}}$. For simplicity, it is assumed that only $\mathrm{V_{Al}}$ and $\mathrm{Al_{Gd}}$ defects are present in significant concentrations, although the following analysis is easily generalized to include $\mathrm{V_{Gd}}$ and $\mathrm{Gd_{Al}}$ defects. It is assumed also that indium does not dissolve interstitially. It is assumed further that defect concentrations are small and that defects do not interact.

Numbers of defect and nondefect species will be indicated below by N^X_y in which X denotes the species (Al, Gd, In or V for vacancy) and y denotes the sublattice or site. N^X denotes the total number of atoms or vacancies X, and N_y the total number of sites of sublattice y. Using N to represent the total number of unit cells, the free energy of the crystal can be written as

$$G=Ng_0+N^{\mathrm{Al}}_{\mathrm{Gd}}g^{\mathrm{Al}}_{\mathrm{Gd}}+N^{\mathrm{V}}_{\mathrm{Al}}g^{\mathrm{V}}_{\mathrm{Al}}+N^{\mathrm{In}}_{\mathrm{Gd}}g^{\mathrm{In}}_{\mathrm{Gd}}+N^{\mathrm{In}}_{\mathrm{Al}}g^{\mathrm{In}}_{\mathrm{Al}}-kT\ln\Omega, \tag{A1}$$

in which g_0 is the Gibbs free energy of the crystal per unit cell in the absence of defects, g^X_y is the free energy of defect X on sublattice y, and Ω is the number of possible ways to arrange the defects,

$$\Omega=\frac{N_{\mathrm{Al}}!N_{\mathrm{Gd}}!}{N^{\mathrm{Al}}_{\mathrm{Al}}!N^{\mathrm{V}}_{\mathrm{Al}}!N^{\mathrm{In}}_{\mathrm{Al}}!N^{\mathrm{Gd}}_{\mathrm{Gd}}!N^{\mathrm{Al}}_{\mathrm{Gd}}!N^{\mathrm{In}}_{\mathrm{Gd}}!}. \tag{A2}$$

The free energy of a defect $g^X_y=h^X_y-Ts^X_y$ is defined as the difference between the free energy of a crystal containing one defect X_y and the perfect crystal at temperature T, for which h^X_y is the difference in enthalpy and s^X_y is the difference in vibrational entropy.

When minimizing the Gibbs free energy with respect to the N's that appear in the above equations, the N's cannot be varied independently. First, the composition of the compound dictates that the ratio of numbers of Gd and Al atoms satisfies

$$\frac{N^{\mathrm{Gd}}}{N^{\mathrm{Al}}}=\frac{N^{\mathrm{Gd}}_{\mathrm{Gd}}}{N^{\mathrm{Al}}_{\mathrm{Al}}+N^{\mathrm{Al}}_{\mathrm{Gd}}}=\frac{1+3x}{2-3x}. \tag{A3}$$

Second, the numbers of sublattice sites must satisfy $2N_{\mathrm{Gd}}=N_{\mathrm{Al}}$, so that

$$2N^{\mathrm{Gd}}_{\mathrm{Gd}}+2N^{\mathrm{Al}}_{\mathrm{Gd}}+2N^{\mathrm{In}}_{\mathrm{Gd}}=N^{\mathrm{Al}}_{\mathrm{Al}}+N^{\mathrm{V}}_{\mathrm{Al}}+N^{\mathrm{In}}_{\mathrm{Al}}. \tag{A4}$$

Since indium concentrations were negligible in the PAC experiments, we neglect the numbers of In atoms in Eq. (A4) to obtain a simpler equation of constraint,

$$2N^{\mathrm{Gd}}_{\mathrm{Gd}}+2N^{\mathrm{Al}}_{\mathrm{Gd}}=N^{\mathrm{Al}}_{\mathrm{Al}}+N^{\mathrm{V}}_{\mathrm{Al}}. \tag{A5}$$

Finally, the choice of a canonical ensemble requires that the numbers of Gd and Al atoms be fixed. For the defect model assumed here, Gd atoms are found only on the Gd sublattice, so that a third constraint can be expressed simply as

$$N^{\mathrm{Gd}}_{\mathrm{Gd}}-N^{\mathrm{Gd}}=0. \tag{A6}$$

Equation (A3) in conjunction with Eq. (A6) constrains the number of Al atoms.

With the above three constraints [Eqs. (A3), (A5), and (A6)], one can obtain the conditions of equilibrium using the Lagrange method of undetermined multipliers. A system of

equations in terms of Lagrange multipliers results, and elimination of the multipliers leads to numerous equations that relate defect concentrations to energies. One is

$$\frac{[V_{Al}]^3[Al_{Gd}]}{[Al_{Al}]} = \exp(-(g_0 + 3g_{Al}^{V} + g_{Gd}^{Al})/k_BT) \equiv \exp(-G_4/k_BT) \equiv K_4, \quad \text{(A7)}$$

in which $[X_y]$ is the fraction of sites on sublattice y occupied by defect or nondefect species X, that is $[X_y] \equiv N_y^X/N_y$. Equation (A7) describes thermal activation of quadruple defects, composed of 3 V_{Al} and 1 Al_{Gd} elementary defects, and can be represented by the reaction

$$Al_{Al} \rightleftarrows 3\ V_{Al} + Al_{Gd}, \quad \text{(A8)}$$

in which the left-hand side represents the perfect lattice and the right-hand side is a quadruple defect. In Eq. (A7), $G_4 \equiv H_4 - TS_4$ is the change in free energy of the crystal when a quadruple defect is formed, including a change in enthalpy H_4 and a change in vibrational entropy S_4. The unit cell energy g_0 appears in (A7) because the right-hand side of reaction (A8) includes one more unit cell than the left-hand side.

A second equation that relates defect concentrations to energies is

$$\frac{[In_{Al}][Al_{Gd}]}{[In_{Gd}][Al_{Al}]} = \exp(-(g_{Al}^{In} - g_{Gd}^{In} + g_{Gd}^{Al})/k_BT) \equiv \exp(-G_{xfer}/k_BT), \quad \text{(A9)}$$

which describes equilibration of indium solutes between Gd and Al sublattices and can be represented by

$$In_{Gd} + Al_{Al} \rightleftarrows In_{Al} + Al_{Gd}. \quad \text{(A10)}$$

In Eq. (A9), $G_{xfer} \equiv H_{xfer} - TS_{xfer}$ is the change in free energy of the crystal when indium changes sites, including a change in enthalpy H_{xfer} and a change in vibrational entropy S_{xfer}.

Defect concentrations can be obtained by first rewriting Eq. (A3) in terms of fractional concentrations and by substituting $[Al_{Al}] = 1 - [V_{Al}]$ to obtain

$$3[Al_{Gd}] + 9x = (2 + 6x)[V_{Al}]. \quad \text{(A11)}$$

In the dilute defect concentration limit, $[Al_{Al}] = 1$ may be inserted into Eq. (A7), and the resulting equation can be substituted into Eq. (A11) to rewrite it in terms of a fourth order polynomial in $[Al_{Gd}]^{1/3}$:

$$[Al_{Gd}]^{4/3} + 3x[Al_{Gd}]^{1/3} - (\tfrac{2}{3} + 2x)K_4^{1/3} = 0. \quad \text{(A12)}$$

Equation (A12) can be solved numerically to determine the Al_{Gd} concentration for given values of x, H_4, and S_4.

According to Eq. (A12), Al_{Gd} is the "structural" defect that must be present at 0 K and for $x<0$ in order to accommodate the deviation from stoichiometry while preserving the crystal structure. It is useful to examine how its concentration changes with temperature and composition. At the stoichiometric composition, $x=0$, there are no structural defects and Al_{Gd} defects are formed solely by thermal activation; from Eq. (A12), $[Al_{Gd}] = (2/3)^{3/4}K_4^{1/4}$. For nonstoichiometric compositions at a sufficiently high temperature that the majority of Al_{Gd} defects are thermally activated, the solution is still approximately $[Al_{Gd}] = (\tfrac{2}{3})^{3/4}K_4^{1/4}$. At low temperatures, the behavior of $[Al_{Gd}]$ differs significantly on either side of stoichiometry. For $x<0$, $[Al_{Gd}] \cong -3x$. For $x>0$, Al_{Gd} defects are only thermally activated and compensate V_{Al} defects (V_{Al} is the structural defect for $x>0$), in which case $[Al_{Gd}] \cong (2/9x)^3K_4$ is found to satisfy Eq. (A7).

Equation (A9) links the ratio of concentrations of indium solutes on each sublattice to the concentration of Al_{Gd} defects according to $[In_{Gd}]/[In_{Al}] = [Al_{Gd}]\exp(G_{xfer}/k_BT)$. Considering the temperature and composition dependence of $[Al_{Gd}]$ just described, for nonstoichiometric compositions at sufficiently high temperature, the ratio will be thermally activated with an activation enthalpy equal to H_{xfer}-$H_4/4$ and prefactor that is effectively independent of sample composition. At low temperature, the ratio will also be thermally activated, but with an activation enthalpy that differs on the two sides of the stoichiometric composition: H_{xfer} for $x<0$ and H_{xfer}-H_4 for $x>0$. Furthermore, the prefactors at low temperature will vary as a function of composition.

*Electronic address: collins@wsu.edu

[1] P. Chartier *et al.*, J. Appl. Phys. **75**, 3842 (1994).
[2] Y. L. Hao *et al.*, Intermetallics **8**, 633 (2000).
[3] M. O. Zacate and G. S. Collins, Hyperfine Interact. **136/137**, 647 (2001).
[4] M. O. Zacate and G. S. Collins, Phys. Rev. B (to be published).
[5] P. Wodniecki *et al.*, Phys. Lett. A **288**, 227 (2001).
[6] G. S. Collins and Matthew O. Zacate (unpublished).
[7] G. S. Collins and M. O. Zacate, Hyperfine Interact. **136/137**, 641 (2001).
[8] H. Jacobi and H.-J. Engell, Acta Metall. **19**, 701 (1971).
[9] C. Woodward, S. Kajihara, and L. H. Yang, Phys. Rev. B **57**, 13459 (1998).
[10] Y. P. Wu *et al.*, Acta Metall. **37**, 2835 (1989).
[11] A. V. Ruban and H. L. Skriver, Phys. Rev. B **55**, 856 (1997).
[12] G. L. Catchen, J. M. Adams, and T. M. Rearick, Phys. Rev. B **46**, 2743 (1992).
[13] P. Villars and L. D. Calvert, *Pearson's Handbook of Crystallographic Data for Intermetallic Phases*, 2nd ed. (ASM International, Materials Park, OH, 1991).
[14] G. F. Zhou and H. Bakker, Phys. Rev. B **52**, 9437 (1995).
[15] I. W. Modder, M. J. Kuin, and H. Bakker, Intermetallics **6**, 537 (1998).
[16] K. A. Gschneidner, Jr. and F. W. Calderwood, in *Binary Alloy Phase Diagrams*, 2nd ed., edited by T. B. Massalski (ASM International, Materials Park, OH, 1990), Vol. 1, p. 151.
[17] F. Sommer and M. Keita, J. Less-Common Met. **136**, 95 (1987).
[18] C. Colinet *et al.*, Physica B **150**, 397 (1988).
[19] Other rare earth compounds studied in this laboratory also gained mass during anneals in H_2 but not in high vacuum. Analyses of composition and mass changes indicated that fractions of rare earth element were lost from the intermetallic compound to form

rare earth oxide.
[20] D. Wegner, Hyperfine Interact. **23**, 179 (1985).
[21] Bin Bai, Ph.D. dissertation, Washington State University, 1998.
[22] M. O. Zacate and G. S. Collins (unpublished).
[23] P. C. Lopiparo and R. L. Rasera, in *Angular Correlations in Nuclear Disintegration*, edited by H. van Krugten and B. van Nooijen (Rotterdam University Press, Groningen, 1971), p. 66.
[24] M. E. Phillips and F. A. Smith, Nucl. Instrum. Methods **165**, 83 (1979).
[25] A. R. Arends *et al.*, Hyperfine Interact. **8**, 191 (1980).
[26] S. N. Mishra *et al.*, Phys. Lett. **91A**, 193 (1982).
[27] Z. Z. Aksel'rod *et al.*, Izv. Akad. Nauk SSSR, Ser. Fiz. **50**, 2372 (1986).
[28] M. Forker *et al.*, J. Magn. Magn. Mater. **226-230**, 1156 (2001).
[29] For a nonstoichiometric composition, point defects must be present in order to preserve the correct ratio of lattice sites and maintain a single phase. These defects are referred to as structural defects, and their concentrations increase with the magnitude of the deviation from stoichiometry.
[30] G. S. Collins and M. O. Zacate, Hyperfine Interact. **151**, 77 (2003).
[31] G. S. Collins, P. Sinha, and M. Wei, Hyperfine Interact. **C1**, 380 (1996).
[32] M. O. Zacate and G. S. Collins, Defect Diffus. Forum **194-199**, 383 (2001).
[33] G. S. Collins, L. S.-J. Peng, and M. O. Zacate, Defect Diffus. Forum **213-215**, 107 (2003).